Drug Delivery and Translational Research (2024) 14:2712–2726
https://doi.org/10.1007/s13346-024-01521-0

ORIGINAL ARTICLE

Stimuli-responsive magnetic silica-poly-lactic-co-glycolic acid hybrid nanoparticles for targeted cancer chemo-immunotherapy

Anuradha Gupta[1,3] · Karishma Niveria[2] · Hitesh Harsukhbhai Chandpa[5] · Mamta Singh[3] · Vikas Kumar[4] · Amulya Kumar Panda[3] · Jairam Meena[5,3]

Accepted: 12 January 2024 / Published online: 12 February 2024

Abstract

Chemotherapy and immunotherapy are two important modalities in cancer management. However, due to multiple reasons, a monotherapy is only partially effective. Hence, if used concurrently in targeted and stimuli-responsive manner, it could have been superior therapeutically. To facilitate co-delivery of chemotherapeutic and immunotherapeutic agent to the target cancer cells, engineered nanoparticles, i.e., a pH-responsive polymer PLGA-coated magnetic silica nanoparticles (Fe_3O_4-SiO_2-PLGA-PDA-PTX-siRNA NPs) encapsulating paclitaxel (PTX) and siRNA against programmed cell death ligand-1 (PD-L1) are synthesized and characterized. Developed nanoparticles demonstrated pH-sensitive sustained drug release up to 10 days. In vitro 4T1 cell line studies showed efficient cellular uptake, PD-L1 gene downregulation, and apoptosis. Further, in vivo efficacy studies carried out in the mice model demonstrated a significant reduction of tumor growth following treatment with dual-Fe_3O_4-SiO_2-PLGA-PDA-PTX-siRNA NPs as compared with monotherapy with Fe_3O_4-SiO_2-PLGA-PDA-PTX NPs. The high therapeutic efficacy observed with dual-Fe_3O_4-SiO_2-PLGA-PDA-PTX-siRNA NPs was mainly due to the cytotoxic effect of PTX combined with targeted silencing of the gene of interest, i.e., PD-L1, which in turn improve $CD8^+$ T cell-mediated cancer cell death as evident with increased proliferation of $CD8^+$ T cells in co-culture experiments. Thereby, dual-Fe_3O_4-SiO_2-PLGA-PDA-PTX-siRNA NPs may have a promising anti-cancer treatment potential against breast cancer; however, the beneficial effects of dual loading of PTX + PD-L1 siRNA may be corroborated against other cancer models such as lung and colorectal cancer models as well as in clinical trials.

Keywords Paclitaxel · Immunotherapy · Programmed cell death ligand-1 (PD-L1) · Small-interfering RNA (siRNA) · Magnetic- silica nanoparticles · Poly-lactic co-glycolic acid (PLGA) · Polydopamine (PDA)

Introduction

An improvement in our understanding of genomics and cell biology led to the advancement of various therapeutic modalities for cancer treatment. The arsenals to treat cancers are chemotherapies, radiotherapies, surgery, hormonal therapy, cell-based therapies, and immunotherapies. The cytotoxic anti-cancer drugs, inhibit DNA/RNA synthesis, induce DNA strand break, and/or interfere with tubulin/microtubule network [1]. Paclitaxel (PTX), a chemotherapeutic agent, has extensively used for the treatment of breast cancer, non-small cell lung cancer, ovarian cancer, malignant tumor, and a variety of solid tumors. However, drug-resistance, low water solubility, and significant toxicities such as peripheral neuropathy and myelosuppression limited its effectiveness [2]. In order to overcome these limitations, various nano-based drug delivery systems such

✉ Jairam Meena
jairam.phe@itbhu.ac.in

1 School of Material Science and Technology, Indian Institute of Technology (BHU) Varanasi, Varanasi 221005, India

2 Nanobiotech Lab, Department of Zoology, Kirori Mal College, University of Delhi, Delhi 110007, India

3 Product Development Cell, National Institute of Immunology, Aruna Asaf Ali Marg, New Delhi 110067, India

4 Cell Biology Lab, Kusuma School of Biological Sciences, Indian Institute of Technology, New Delhi 110067, India

5 ImmunoEngineering and Therapeutics Laboratory, Department of Pharmaceutical Engineering and Technology, Indian Institute of Technology (BHU) Varanasi, Varanasi 221005, India

as nanoparticle albumin-bound paclitaxel (Nab-PTX), polymeric micelles encapsulating paclitaxel, polymer-paclitaxel conjugates, liposomal paclitaxel, and many more have been developed [3].

Killing cancer cells using a single chemotherapeutic agent may often lead to the emergence of drug resistance or relapse of tumor. Consequently, immunotherapy has advanced cancer treatment regimen, displaying high therapeutic potential. Several oligonucleotide-based immunotherapies have been explored alone or in combination with chemotherapeutic agents [4–6]. Of note, DNAzymes have inspired the research fraternity due to its multiple advantages including higher targeting ability, higher stability, easy and cheaper to synthesize. However, presence of metal co-factors, target substrate chain length, and presence of other enzymes in the solution can influence the DNAzymes catalytic rate and limit its therapeutic use [7]. Thereby, the siRNA-based gene silencing strategy has widely been explored and has shown its promise in preclinical and clinical studies. Recently, immunotherapies directed at immune check point inhibitors PD-1/PD-L1 (programmed cell death protein-1/programmed cell death-ligand1) interactions have been exploited to prevent immune escape mechanisms of cancer cells. Over expression of immune checkpoint inhibitor PD-L1 (a ligand of PD-1) on tumor cells inhibits the activation of T cells upon binding to its receptor PD-1 (programmed cell death protein-1) [8]. Thereby, small-interfering RNA (siRNA) mediated post-transcriptional gene silencing of PD-L1 has demonstrated anti-cancer therapeutic potential, However, systemic delivery of PD-L1 siRNA also suffers with the limitations of degradation by nucleases; presenting a very short half-life of 15 min to 1 h in circulation, off-target effects, and reduced cancer cell uptake [9, 10].

Furthermore, to overcome the limitations associated with siRNA use, delivery systems, i.e., viral vector and polymeric nanoparticles were used. However, due to various advantages associated with polymeric nanoparticles specifically, the enhanced half-life of siRNA in blood, better targeting due to enhanced permeation and retention (EPR) effect, improved pharmacokinetics, its non-immunogenic nature compared to viral vectors, and superior safety profile have had made nanoparticle-based gene delivery as the preferred choice for cancer therapy [11–13].

It is generally acknowledged that cancer cannot be treated effectively with one therapeutic modality [1, 14, 15]. Therefore, potentiating tumor-specific immune response along with chemotherapy may ablate the tumor effectively. The combined use of paclitaxel and PD-L1 siRNA for the treatment of cancer has not been explored too much because of targeting and delivery concerns. For the purpose of co-delivering chemotherapeutic drug and siRNA to tumor cells, active/passive tumor targeting strategies via nanoparticles have been explored with increased cellular uptake, specific tumor homing, and retention with high intracellular concentration of cargo molecule [16, 17]. Thiramanas et al. have developed silica core-shell nanocapsules (~ 240 nm in size), carrying PD-L1 siRNA to knockdown PD-L1 expression in T cells and demonstrated a decrease in PD-L1 protein and mRNA level leading to enhanced T cell survival [18]. Wu et al. have synthesized lipid-coated calcium phosphate nanoparticles encapsulating siRNA against PD-1 and PD-L1, which resulted in an increase in tumor-infiltrating lymphocyte (TIL)-mediated cytotoxicity to cancer cells [19]. Similarly, iron oxide nanoparticles (Fe_3O_4 or γ-Fe_2O_3) [20–22], core-shell structural magnetic mesoporous nanoparticles (Fe_3O_4-SiO_2) [23], iron oxide coated with three polymeric shells have also shown great potential in delivering LCS-1 (a pyridazin-3-one derivative, a well-known inhibitor of superoxide dismutase 1) [24], and niclosamide [25] with promising anti-cancer efficacy.

Surface-modified iron oxide silica nanoparticles have garnered special attention owing to iron-mediated superparamagnetic, magnetic targeting, optical detectability, easy synthesis, and separation properties, whereas silica nanoparticles offered mesoporous structure enabling high loading efficiency, external surface functionalization, and high dispersibility. Organic polymers such as poly (D,L-lactic-co-glycolic acid) (PLGA) are well-known drug delivery polymers, conveying efficient drug encapsulation, sustained/controlled drug release, biocompatible, and biodegradable properties.

Hence, we posit the fabrication of engineered nanoparticles, i.e., Fe_3O_4-SiO_2-PLGA-PDA NPs that have the attributes of targeting via external magnetic navigation to the tumor and releasing the therapeutics PTX and PD-L1 siRNA "on-demand" in a spatio-temporally controlled fashion in tumor cells, minimizing off-target effects and may exert combined/synergistic anti-cancer effect. This combined treatment approach may lead to decreased proliferation and reduction in survival of cancer cells by exerting paclitaxel mediated cancer cell killing along with siRNA-mediated programmed death ligand-1 receptor (PD-L1) downregulation which is overexpressed by tumor cells.

Material and methods

Chemicals, reagents, and antibodies

Paclitaxel (PTX) (CAS number 33069-62-4), tetraethyl orthosilicate (TEOS), sodium hydroxide (NaOH), and dopamine hydrochloride (dopamine HCl) were purchased from Sisco Research Laboratories Pvt. Ltd. India. Polyvinyl alcohol (PVA, 30–70 kDa), dimethyl sulfoxide (cell culture grade), and esiRNA targeting mouse Cd274 (esiRNA1)/PDL1 gene (EMU046161) were purchased

from Sigma-Aldrich/Merck, USA. Iron (III) chloride hexahydrate ($FeCl_3.6H_2O$), iron (II) chloride tetrahydrate ($FeCl_2.4H_2O$), 3-aminopropyl triethoxysilane (APTES), ethanol, and dichloromethane were procured from Merck, India. Poly (D,L-lactic-co-glycolic acid) (50:50) was procured from Purac Biochem, Holland. Tris hydrochloride was procured from Amresco, USA. CyQUANT MTT cell viability assay kit, Lipofectamine 2000 transfection reagent, CD274 (PD-L1, B7-H1) monoclonal Antibody (MIH5), PE, eBioscience™ (Cat #12–5982-82); CD3 monoclonal antibody (17A2), eFluor™ 450, eBioscience™ (Cat # 48–0032-82), CD8a monoclonal antibody (53–6.7), APC, eBioscience™ (Cat # 17–0081-82), and Cell Trace™ CFSE cell proliferation kit (Cat # C34554) were purchased from Thermo Fisher Scientific. RPMI-1640, fetal calf serum and TEM grids, and 6-Coumarin were purchased from Himedia laboratories, India, and Polysciences, USA respectively.

Synthesis of pH-responsive PLGA-coated core-shell magnetic silica nanoparticles

Dopamine-capped PLGA-tethered magnetic silica nanoparticles (Fe_3O_4-SiO_2-PLGA-PDA NPs) were synthesized in four steps. In brief, iron oxide nanoparticles (Fe_3O_4 NPs) were prepared in first step by co-precipitation of iron (II) and iron (III) salts under basic conditions using 2M NaOH [26]. Then, Fe_3O_4 NPs were coated with silica using the modified sol-gel homogenous co-precipitation process to synthesize core-shell magnetic silica nanoparticles (Fe_3O_4-SiO_2 NPs) and amine functionalized [27]. In the third step, these nanoparticles were coated with polymer PLGA to encapsulate paclitaxel and/or PD-L1 siRNA using a double emulsion solvent evaporation method, and Fe_3O_4-SiO_2-PLGA NPs were synthesized [28].

In order to load cargo molecule and prepare paclitaxel-loaded nanoparticles (Fe_3O_4-SiO_2-PLGA-PDA-PTX NPs), 13 mg PTX and 50 mg of polymer PLGA were dissolved in 1 ml and 4 ml of dichloromethane (DCM) respectively and mixed. Fifty milligrams of Fe_3O_4-SiO_2 NPs were dispersed in 0.5 ml of 1% PVA solution and added to PLGA solution with probe sonication (30% amplitude, 20 duty cycles, 2 min) to form primary emulsion (W_1/O). Thus, formed W_1/O emulsion was then added to 30 ml of 2% PVA solution with sonication (30% amplitude, 20 duty cycles, 3 min) to form a double emulsion (W_1/O/W_2) and continuously stirred for 5 h to evaporate DCM. After 5 h, PLGA-coated nanoparticles designated as Fe_3O_4-SiO_2-PLGA-PTX NPs were collected using external magnet and coated with PDA.

Likewise, to prepare PD-L1 siRNA-loaded nanoparticles (Fe_3O_4-SiO_2-PLGA-PDA-siRNA NPs), siRNA stock solution was prepared in nuclease-free water as per manufacturer's instructions. The theoretical load of siRNA was 0.6 µg/mg of NPs. Thereby, to prepare 10 mg of Fe_3O_4-SiO_2-PLGA-PDA-siRNA NPs, 6 µg of siRNA was mixed with 0.25 ml of 5 mg of Fe_3O_4-SiO_2 NPs and PLGA (5 mg) was dissolved in 2.5 ml DCM. Then, W_1/O emulsion was prepared by adding siRNA-Fe_3O_4-SiO_2 NPs to PLGA solution with probe sonication. Thus, prepared primary emulsion was then added to 10 ml of 2% PVA solution with solution and magnetically stirred for 5 h to evaporate DCM. Thus, obtained siRNA-loaded NPs were collected, washed, and coated with polydopamine, lyophilized, and stored at − 20 °C. Similarly, dual-PTX and PD-L1 siRNA-loaded nanoparticles were prepared.

Polydopamine (PDA) [29], a pH-responsive gatekeeper with open-close transformation [30], was capped on these nanoparticles to fabricate pH-responsive system designated as Fe_3O_4-SiO_2-PLGA-PDA-PTX NPs, Fe_3O_4-SiO_2-PLGA-PDA-siRNA NPs, and dual-Fe_3O_4-SiO_2-PLGA-PDA-PTX-siRNA NPs [9]. Figure 1 shows the complete synthetic procedure and the detailed synthetic procedure is mentioned in Supplementary methods.

Characterization of nanoparticles

The nanoparticles were characterized at each step by Fourier transform infrared (FT-IR) spectroscopy, UV-Vis spectroscopy, transmission electron microscopy (TEM), and Malvern zeta sizer. FT-IR spectra of nanoparticles were recorded in the range of 4000–400 cm^{-1} using Thermo

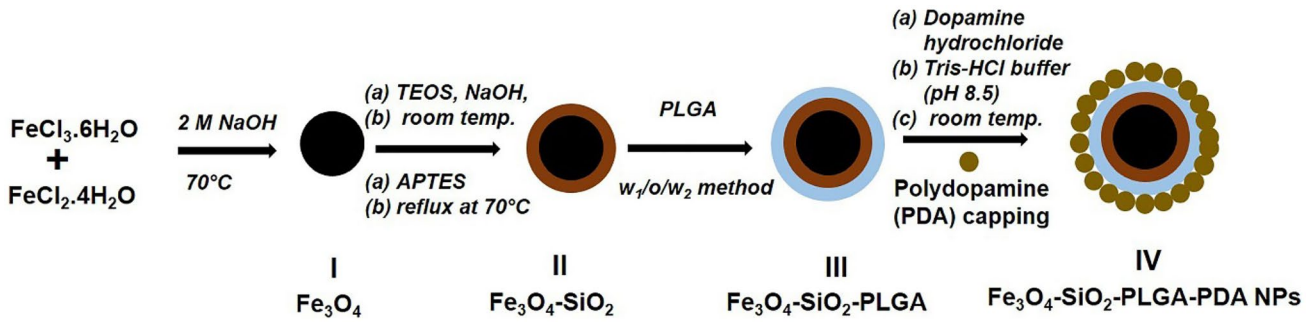

Fig. 1 Step-wise synthesis of layer-by-layer PDA-capped Fe_3O_4-SiO_2-PLGA NPs

Scientific Nicolet iS5 spectrometer with KBr pellet technique. UV-Vis absorption spectra were reported in the wavelength range of 185–900 nm using UV-Vis spectrophotometer (UV-2600i, Shimadzu Corporation, Japan). The mean hydrodynamic diameter, size distribution, and zeta potential of nanoparticles were determined in distilled water using Malvern zeta sizer (Zeta sizer Nano series, Malvern Instruments Ltd., UK) at a wavelength of 633 nm with a scattering angle of 90°. The morphology, size, and coating of PLGA on Fe_3O_4-SiO_2-PLGA-PDA NPs were observed using transmission electron microscopy (TEM) (Technai TEM G^2, Holland). The samples for TEM analysis were prepared on carbon-coated copper grids.

Loading and encapsulation efficiency

To determine PTX loading, 5 mg of dual-Fe_3O_4-SiO_2-PLGA-PDA-PTX-siRNA NPs was dissolved in DCM followed by addition of methanol. The mixture was centrifuged at 15,000 *g* for 20 min, supernatant was collected, vacuum dried, and reconstituted in methanol. The amount of drug was estimated using UV-Vis spectroscopy at a λmax of 230 nm.

To calculate siRNA loading and encapsulation efficiency, 5 mg of dual-Fe_3O_4-SiO_2-PLGA-PDA-PTX-siRNA NPs was dissolved in 200 µl of chloroform followed by the addition of 1 ml of Tris-EDTA (TE) buffer and gently mixed. Then, the mixture was centrifuged at 15,000 *g* for 20 min to collect aqueous phase. PD-L1 siRNA concentration in the aqueous phase was determined using Nano Drop at a λmax of 260 nm. Loading capacity and encapsulation efficiency of PTX and PD-L1 siRNA were calculated using Eqs. (1) and (2) respectively.

$$loading\ capacity = \frac{Amount\ of\ drug/siRNA\ in\ nanoparticles}{Total\ amount\ of\ nanoparticles} \quad (1)$$

$$\%\ encapsulation\ efficiency = \frac{Total\ amount\ of\ drug/siRNA - Amount\ of\ free\ drug/siRNA}{Total\ amount\ ofdrug/siRNA} \times 100 \quad (2)$$

pH-mediated paclitaxel release from PTX-loaded nanoparticles

To observe pH-sensitive release properties, PTX release studies were performed in 10 mM phosphate-buffered saline (PBS) using PDA-coated Fe_3O_4-SiO_2-PLGA-PDA-PTX NPs and uncoated Fe_3O_4-SiO_2-PLGA-PTX NPs at pH 7.4 (blood pH) and 6.0 (tumor pH). Approximately 15 mg NPs were suspended in 1 ml of PBS and packed in dialysis tubes with a molecular weight cutoff of 12 kDa. The dialysis bag was placed in 50 ml of the release media (PBS). Samples were withdrawn at regular intervals for 10 days and sink conditions were maintained. Absorbance and drug content were measured using UV-visible spectroscopy at a λmax of 230 nm and % cumulative drug release vs. time graph was plotted to determine the pH-sensitive PTX release profile.

Cell line and cell culture

4T1 cells (breast cancer cell line derived from the mammary gland tissue of a mouse BALB/c) were generously provided by Dr. Avinash Bajaj (Regional Centre for Biotechnology, Faridabad, India). Cells were cultured in RPMI-1640 medium containing 10% fetal bovine serum in a CO_2 incubator maintained at 37 °C in an atmosphere containing 5% CO_2.

Intracellular uptake of particles

The cellular uptake of the FITC-BSA-loaded Fe_3O_4-SiO_2-PLGA-PDA NPs was demonstrated by flow cytometry (BD-FACS Calibur). In brief, 4T1 cells (1×10^6) were seeded in 6-well plate and allowed to grow for 12 h in a CO_2 incubator at 37 °C. Then, fluorescent nanoparticles containing trace amount of dye (FITC-BSA) was added at a concentration of 25 and 50 µg/ml and incubated for 3 h. Cells were washed with PBS to remove the unbound NPs and collected with the help of cell scraper. After collection, cells were centrifuged at 1200 rpm for 5 min and resuspended in 400 µl of PBS. Flow cytometry analysis was carried out employing an FL-2 detector and the results were expressed as shift in histogram toward higher intensity side. Trypan blue dye was added in the cell's suspension before analysis by flow cytometry to quench the fluorescence associated with membrane interacting nanoparticles and dead cells.

Endonuclease protection assay

In order to observe the siRNA-loaded nanoparticles mediated protection of PD-L1 siRNA from endonuclease digestion, RNase A protection assay was performed. Briefly, soluble PD-L1 siRNA and PD-L1 siRNA NPs containing equivalent amount of siRNA were incubated with RNase A (30 µg/ml) for 4 h at 37 °C. After incubation, PD-L1 siRNA was extracted from NPs. To extract siRNA, NPs were dissolved in chloroform and TE buffer was added. The aqueous phase was removed by centrifugation and 2% agarose gel electrophoresis was run using ethidium bromide staining. PD-L1 siRNA without RNase A treatment was used as experimental control.

In vitro silencing of PD-L1 gene using PD-L1 siRNA-loaded nanoparticles

PD-L1 siRNA NP-mediated knockdown of PD-L1 gene was observed by flow cytometry and quantitative real-time PCR (qRT-PCR) analysis. Initially, 4T1 cells were seeded in 6-well plate at a density of 1×10^6 cells per well. After 24 h, cells were treated with lipofectamine/PD-L1 siRNA (100 nM) and PD-L1 siRNA NPs for 6 h ($n = 3$). Extracellular NPs were removed by washing with PBS and incubated for additional 16 h. For flow cytometry, cells were fixed with 4% paraformaldehyde, permeabilized with 0.25% Triton X-100 at 37 °C for 15 min, and washed with PBS. The cells were then incubated with anti-mouse D274 (PD-L1, B7-H1) monoclonal antibody (MIH5), PE (dilution 1:50), overnight at 4 °C, washed, and resuspended in 0.5 ml PBS. After that, cells were analyzed by flow cytometry, and untreated cells were taken as experimental control.

To perform qRT-PCR analysis, following 48 h of treatment ($n = 3$), total RNA was harvested by the TRIzol (Invitrogen) method. cDNA was prepared from 0.5 µg of total RNA using one iScript cDNA synthesis kit (Bio Rad, USA) as per manufacturer's instructions. Target gene PD-L1 expression level was analyzed using gene-specific primers (forward 5′-GGAATTGTCTCAGAATGGTC-3′ and reverse 5′-GTA GTTGCTTCTAGGAAGGAG-3′) at a specific condition of 50 °C (2 min) and 94 °C (10 min) followed by 40 cycles of 95 °C (15 s) and 56 °C (60 s) using ABI QuantStudio5 (Applied Biosystems). GAPDH was taken as internal control for each experiment (forward 5′-CAAGATCATCAGCAATGCCT-3′ and reverse 5′-GCCATCACGCCACAGTTTCC-3′). Threshold cycle (Ct value) was calculated and mRNA expression of PD-L1 gene was quantified using the $2^{-\Delta\Delta Ct}$ method where $\Delta\Delta C_t = \Delta C_t$ target gene $- \Delta C_t$ GAPDH.

Hemocompatibility study

Hemocompatibility assay was performed to investigate the biocompatibility of nanoparticles with circulating blood cells. The blood was collected from healthy mice with the approval of Institutional Animal Ethics Committee (IAEC#500/19) and red blood cells (RBCs) was separated from blood by centrifugation at 2000 rpm for 5 min. RBCs were washed, resuspended in sterile PBS, and then incubated with NPs at different concentrations of 25, 50, 100, and 200 µg/ml at 37 °C for 4 h. After 4 h of incubation, the samples were centrifuged at 2500 rpm for 5 min, and supernatant was collected. The supernatant was analyzed by UV-visible spectroscopy at λmax of 540 nm and % hemolysis was calculated using Eq. (3). RBCs incubated with 0.1% triton X-100 and sterile PBS were taken as positive and negative control, respectively. The experiments were performed in triplicate and data are represented as mean ± standard deviation of three independent sets of experiments.

$$\%\ hemolysis = \frac{absorbance\ of\ each\ sample - absorbance\ of\ negative\ control}{absorbance\ of\ positive\ control - absorbance\ of\ negative\ control} \times 100 \quad (3)$$

Cytotoxicity assay

3-(4,5-Dimethylthiazol-2-yl)-2,5-diphenyltetrazolium bromide (MTT) assay was performed to determine the killing efficacy of Fe_3O_4-SiO_2-PLGA-PDA-PTX NPs vs. PTX solution against 4T1 cells. Briefly, cells were seeded in a 96-well culture plate (5×10^3 cells/well), treated with PTX solution and Fe_3O_4-SiO_2-PLGA-PDA-PTX NPs with or without PD-L1 siRNA for 48 h. Cells were washed with PBS to remove extracellular NPs. MTT solution (1:10 dilution of 5 mg/ml in PBS) was added to each well and incubated at 37 °C for 4 h. The medium was then removed and 150 µl of dimethyl sulfoxide (DMSO) was added to dissolve the formazan crystals and incubated for 10 min. Absorbance was recorded at the wavelength of 590 nm and 639 nm using a 96-well plate reader (Micro titer plate reader BioTek synergy 2, Finland) and % cell viability and half-maximal inhibitory concentration (IC_{50}) was calculated.

Annexin V-FITC apoptosis assay

4T1 cells (1×10^6 cells/well) were seeded in 6-well and allowed to grow. Cells were treated with PTX drug solution, Fe_3O_4-SiO_2-PLGA-PDA-siRNA NPs, Fe_3O_4-SiO_2-PLGA-PDA-PTX NPs, and dual-Fe_3O_4-SiO_2-PLGA-PDA-PTX NPs at 1 µg/ml concentration. DMSO and bare NPs served as experimental control. After 24 h of treatment, cells were collected with cell scraper, centrifuged, and resuspended in 100 µl of binding buffer. Annexin V-FITC (5µl) and propidium iodide (PI, 1 µl of 100 µg/ml) staining was performed as per manufacturer's protocol and cells were analyzed using flow cytometry using CELLQuest 3.0 software. Where viable cells showed no staining (Annexin V^-, PI^-), while early apoptotic cells, late apoptotic cells and necrotic cells were observed as Annexin V positive (Annexin V^+, PI^-), positive for both dyes (Annexin V^+, PI^+), and PI positive only (Annexin V^-, PI^+), respectively.

Effect of PD-L1 knockdown on $CD8^+$ T cell proliferation

To assess the effect of PD-L1 knockdown on $CD8^+$ T cell proliferation, 4 T1 cells and CFSE-labeled splenocytes co-culture studies were performed using flow cytometry. Initially, BALB/c mice were immunized with 4T1 cell lysate; splenocytes were isolated from the spleen and CFSE labeled. Then, CFSE-labeled splenocytes were co-cultured with 4 T1 cells treated with nanoparticles. The detailed procedure is given below:

Animal immunization for T cell priming

Initially, 4T1 cell lysate was prepared by the freeze–thaw method using 1×10^6 cells and stored at − 70 °C till further use. BALB/c mice were immunized with 50 µl of 4T1 cells lysate per mouse on day 0 and day 7. All the animals were sacrificed on day 14th and spleens were collected. Spleens were gently triturated with the thumb head of sterile syringe plunger and filtered using 70µM cells strainer under the laminar air flow to prepare single-cell suspension. Cell pellet was collected by centrifugation at 1500 rpm for 5 min and RBCs were lysed by resuspending cells in ice-cold ACK lysing buffer and incubating on ice for 5 min. The splenocytes were collected by centrifugation at 1500 rpm for 5 min, counted by hemocytometer, and cultured in RPMI-1640 media containing10% FBS.

CFSE labeling and analysis using flow cytometry

Cell Trace™ CFSE stock solution (5 mM) was prepared by dissolving 1 vial in 18 µl of anhydrous DMSO as per manufacturer instructions. Then, 1 µl of stock solution was added to 1 ml of splenocytes suspension (2×10^6 cells/ml) for a final working concentration of 5 µM, and incubated in dark for 20 min at room temperature. After incubation, splenocytes were centrifuged at 1500 rpm for 5 min at 4 °C, supernatant was removed, and excess dye was removed by washing cells two times with complete RPMI-1640 media.

Co-culture of CFSE-labeled splenocytes with 4T1 cells

PD-L1 receptors were knockdown in the 4T1 cells for the assessment of T cell response in a co-culture of 4T1 tumor cells and splenocytes primed against tumor cells. In brief, 4T1 cells were seeded in a 96-well plate at a density of 0.4×10^5 cells per well. After 12 h, cells were treated with Fe_3O_4-SiO_2-PLGA-PDA-NPs, Fe_3O_4-SiO_2-PLGA-PDA-siRNA NPs, and dual-Fe_3O_4-SiO_2-PLGA-PDA-PTX-siRNA NPs for 6 h. Extracellular NPs were removed by washing with PBS and incubated for additional 6 h. After incubation, cells were washed and used for cancer cells-T cells co-culture assay. In the next step, 0.4×10^5 4T1 cells were co-cultured with 1×10^5 splenocytes in the RPMI-1640 media supplemented with 10% FBS at 37 °C in humidified CO_2 cell culture incubator. After 48 h of incubation, cells were labeled with fluorochrome-tagged antibodies: CD3 monoclonal antibody (17A2), eFluor™ 450, eBioscience™, and CD8a monoclonal antibody (53–6.7), APC, eBioscience™ antibodies as per the manufacturer's instructions, centrifuged, resuspended in PBS, and T cells proliferation was analyzed using CytoFlex flow cytometer (Backman coulter).

Tumor inhibition and animal survival studies

Female BALB/c mice at 6–8 weeks of age were obtained from the Institutional animal facility and allowed to adapt for 1 week and had access to food and water ad libitum. All the animal experiments were performed with the approval of IAEC of National Institute of Immunology, New Delhi, India (IAEC#500/19). In brief, the tumor was developed in female BALB/c mice by a single injection of 0.5×10^6 4T1 cells into left mammary fat pad and tumor growth was monitored. When the tumor was palpable and reached a size of > 100 mm^3, animals were randomly divided into different groups of five animals each: saline, PTX drug solution, Fe_3O_4-SiO_2-PLGA-PDA-PTX NPs, dual-Fe_3O_4-SiO_2-PLGA-PDA-PTX-siRNA NPs, and bare NPs. For therapeutic studies, 8 mg/kg of paclitaxel was given by intraperitoneal injection after 72 h either as drug solutions or as Fe_3O_4-SiO_2-PLGA-PDA-PTX NPs and dual-Fe_3O_4-SiO_2-PLGA-PDA-PTX-siRNA NPs repeatedly for 15 days. Tumor growth inhibition was monitored by calculating the tumor volume, changes in mice body weight during treatment period, and animal survival. The tumor volume (mm^3) was calculated using Eq. (4):

$$tumour\ volume\ (mm^3) = \frac{(width\ of\ tumor \times length\ of\ tumor)^2}{2} \quad (4)$$

Results and discussion

Synthesis of nanoparticles and characterization

Synthesis of nanoparticles was carried out in four steps captivating the three-layered approach (Fig. 1), where each layer aided additional advantage to the engineered nanocarrier. Magnetic core material (Fe_3O_4 NPs) served advantage of magnetic separation during synthesis and removal of chemical contaminants. Furthermore, iron oxide-mediated magnetic targeting properties and hyperthermia media cancer cell killing can be explored later to increase the therapeutic efficacy [31]. The magnetic nanoparticles (Fe_3O_4) prepared

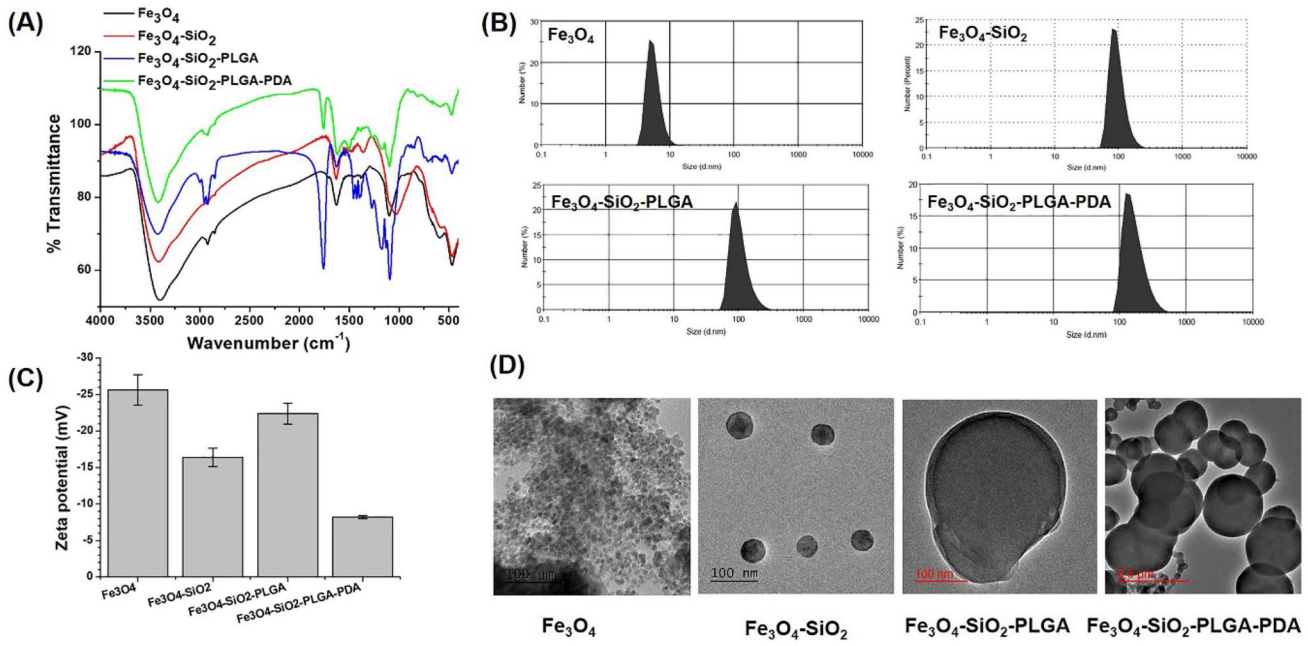

Fig. 2 Characterization of Fe_3O_4 NPs following coating with silica, PLGA, and PDA at each step by **A** FT-IR spectroscopy, **B** particle size distribution, **C** zeta potential, and **D** transmission electron microscopy

in this study were 8–10 nm in size as observed by transmission electron microscopy and zeta sizer and allowed easy separation with external magnet during synthesis (Fig. 2). In the second step, core-shell magnetic silica nanoparticles were prepared using tetra ethyl ortho silicate (TEOS) and (3-aminopropyl) triethoxysilane (APTES) as precursors. The size of magnetic silica nanoparticles (Fe_3O_4-SiO_2 NPs) was measured as 135.33 ± 7.41 nm with zeta sizer. Amine functionalized silica layer assisted in improving the dispersibility of Fe_3O_4 NPs.

In the third step, the second layer of polymer PLGA facilitated PTX drug encapsulation, sustained PTX release up to 8 days (Fig. 3), and improved biocompatibility and biodegradability of nanoparticles. PLGA is FDA-approved polymer, most commonly used for drug delivery applications because of excellent biocompatible and biodegradable properties, providing controlled drug release [32]. In the fourth step, Fe_3O_4-SiO_2-PLGA NPs were capped with polydopamine (PDA) to develop a pH-sensitive targeted delivery system. In the basic conditions, dopamine gets oxidized and polymerized to form a dense shell of PDA on the surface of NPs, thus fabricating a pH-controlled drug delivery system [33]. The three-layer coating on iron oxide was monitored by changes in FT-IR spectra, particle size, zeta potential, and transmission electron microscopy. Figure 2A shows the FT-IR spectra, where iron oxide showed the characteristic peak at 589 cm^{-1}. Silica coating was observed as the presence of additional peaks at 952 and 1020 cm^{-1} corresponding

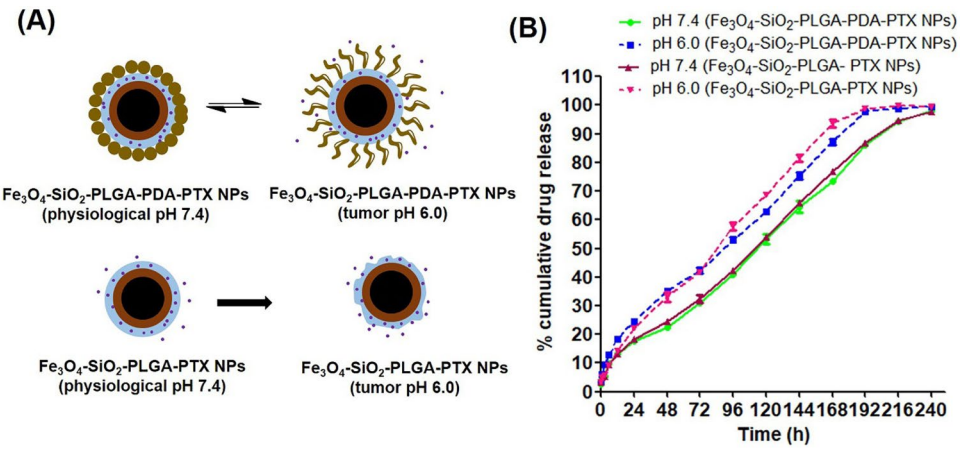

Fig. 3 Paclitaxel release studies: **A** schematic illustration showing PTX release from PDA-coated (Fe_3O_4-SiO_2-PLGA-PDA-PTX NPs) and -uncoated Fe_3O_4-SiO_2-PLGA-PTX NPs at physiological and tumor pH, **B** pH-triggered PTX release by Fe_3O_4-SiO_2-PLGA-PDA-PTX NPs and sustained release profile up to 10 days. Data is represented as mean ± standard deviation, $n = 3$)

to asymmetric stretching of Si-O-Si with Fe_3O_4-SiO_2 NPs. The second layer of PLGA was confirmed in infrared spectroscopy with the presence of small peaks in the range of 2800–3200 cm^{-1} assigned to asymmetric and symmetric stretching vibrations of -CH_2 due to long alkyl chain of glycolic and lactic acid units of PLGA structure. The third layer of PDA on Fe_3O_4-SiO_2-PLGA-PDA NPs was confirmed with the presence of N-H (secondary amine) stretching and bending vibrations at 3480 cm^{-1} and 1604 cm^{-1}. The peak at 3791 cm^{-1} was detected due to -OH group of adsorbed water molecules.

Coating leads to increase in hydrodynamic diameter of nanoparticles. Thereby, particle size analysis (Fig. 2B) showed the increase in size of nanoparticles with the silica, PLGA, and PDA coating on Fe_3O_4 NPs. Dynamic light scattering analysis reported the number distribution particle size of Fe_3O_4, Fe_3O_4-SiO_2, Fe_3O_4-SiO_2-PLGA, and Fe_3O_4-SiO_2-PLGA-PDA NPs as 8.0 ± 3.0 nm, 135.33 ± 7.41 nm, 153.66 ± 10.08 nm, and 225.33 ± 9.84 nm, respectively, which supported the three-layer coating on Fe_3O_4 NPs. While intensity distribution analysis of Fe_3O_4-SiO_2-PLGA-PDA NPs showed the particle size as 262.1 nm with a polydispersity index of 0.26 which suggests that the particles were homogeneous in nature.

Changes in zeta potential also advocates the modification of Fe_3O_4 NPs, initially magnetic nanoparticles showed the negative zeta potential of -25.63 ± 2.08 mV due to presence of the abundant surface hydroxyl group. Further silica coating and PLGA coating led to a change in zeta potential to -16.38 ± 1.23 mV, and -22.36 ± 1.45 mV respectively. Finally, Fe_3O_4-SiO_2-PLGA-PDA NPs reported the zeta potential values as -8.19 ± 0.20 mV due to presence of positively charged amine groups on the NPs surface (Fig. 2C). Finally, Fe_3O_4-SiO_2-PLGA-PDA-PTX NPs, Fe_3O_4-SiO_2-PLGA-PDA-siRNA NPs, and dual-Fe_3O_4-SiO_2-PLGA-PDA-PTX-siRNA NPs displayed the size as 232.33 ± 8.16 nm, 239.67 ± 4.92 nm, 239.0 ± 5.71 nm, and negative zeta potential value as -8.04 ± 0.72, -8.41 ± 0.57, and -8.24 ± 0.35 mV, respectively.

UV spectrum changes were also suggested the magnetic nanoparticles coating with silica, PLGA, and PDA (Supplementary Fig. S1), where Fe_3O_4 showed a broad absorbance spectrum in the wavelength range of 200–500 nm. Silica and PLGA coating led to a decrease in the absorbance of iron oxide. Coating with PDA showed the characteristic peak of dopamine at 282 nm, which confirmed the PDA attachment to the outer surface of Fe_3O_4-SiO_2-PLGA NPs.

Drug loading and release behavior

Paclitaxel loading capacity and encapsulation efficiency of Fe_3O_4-SiO_2-PLGA-PDA-PTX NPs were calculated and estimated as 91.88 ± 1.2 µg/mg and 79.86 ± 1.04%, respectively with UV-Vis spectroscopy. The % encapsulation efficiency of Fe_3O_4-SiO_2-PLGA-PDA-siRNA NPs was 33.83 ± 1.04%, with a siRNA loading capacity of 203 ± 6.24 ng/mg of NPs. To study the effect of PDA coating on pH-sensitive release, PTX release was compared using PDA-coated Fe_3O_4-SiO_2-PLGA-PDA-PTX NPs and uncoated Fe_3O_4-SiO_2-PLGA-PTX NPs at pH 6.0 and pH 7.0.

Figure 3A shows the schematic release from PDA-coated and -uncoated particles. At pH 7.4, PDA prevents the leakage of cargo molecule in release media and likely in systemic circulation also, whereas uncoated Fe_3O_4-SiO_2-PLGA-PTX NPs continue to release in systemic circulation at pH 7.4, thus may induce some side effects. Figure 3B shows % cumulative PTX release vs. time graph. Release studies carried out at pH 6.0 and 7.4 demonstrated only a slight change in drug release at pH 6.0 as compared to pH 7.4 by unlocking the channels at acidic pH by Fe_3O_4-SiO_2-PLGA-PDA-PTX NPs. Only slight change in the drug release profile at two different pH by PDA-coated NPs could be due to thin coating at NPs surface. After 96 h, % cumulative drug release was observed as 52% and 41% at pH 6.0 and 7.4 respectively. Fe_3O_4-SiO_2-PLGA-PDA-PTX NPs also minimized drug leakage during systemic circulation, thus more suitable for preventing PTX-mediated off-target effects. Uncoated particles also displayed pH-dependent release because of faster polymer degradation at acidic pH. However, Fe_3O_4-SiO_2-PLGA-PDA-PTX NPs exhibited more sustained PTX release (98% drug release in 9 days) as compared to uncoated Fe_3O_4-SiO_2-PLGA-PTX NPs (98% drug release in 8 days) because of additional layer of PDA, resulting in increase in polymer swelling time and degradation rate.

Intracellular uptake

Cellular uptake of NPs was investigated by flow cytometry analysis (Fig. 4A). Treatment of 4T1 cells with fluorescent particles (FITC-loaded NPs) at a concentration of 25 and 50 µg/ml resulted in a shift in fluorescent intensity to higher side with 94% and 99% cells positive, respectively. These results suggested that these NPs were efficiently internalized by 4T1 cells within 3 h of treatment. Untreated 4T1 cells were taken as control of autofluorescence. These results suggested that dual-Fe_3O4-SiO_2-PLGA-PDA-PTX-siRNA NPs are able to efficiently deliver PTX and PD-L1 siRNA intracellularly within cancer cells and remarkably reduce the PTX-mediated side effects on normal cells due to cancer cell targeting.

Protection of PD-L1 siRNA from endonuclease

Figure 4 E shows the results of RNase protection assay where there is no band for naked siRNA incubated with RNase-A specifying complete degradation of naked siRNA by nuclease

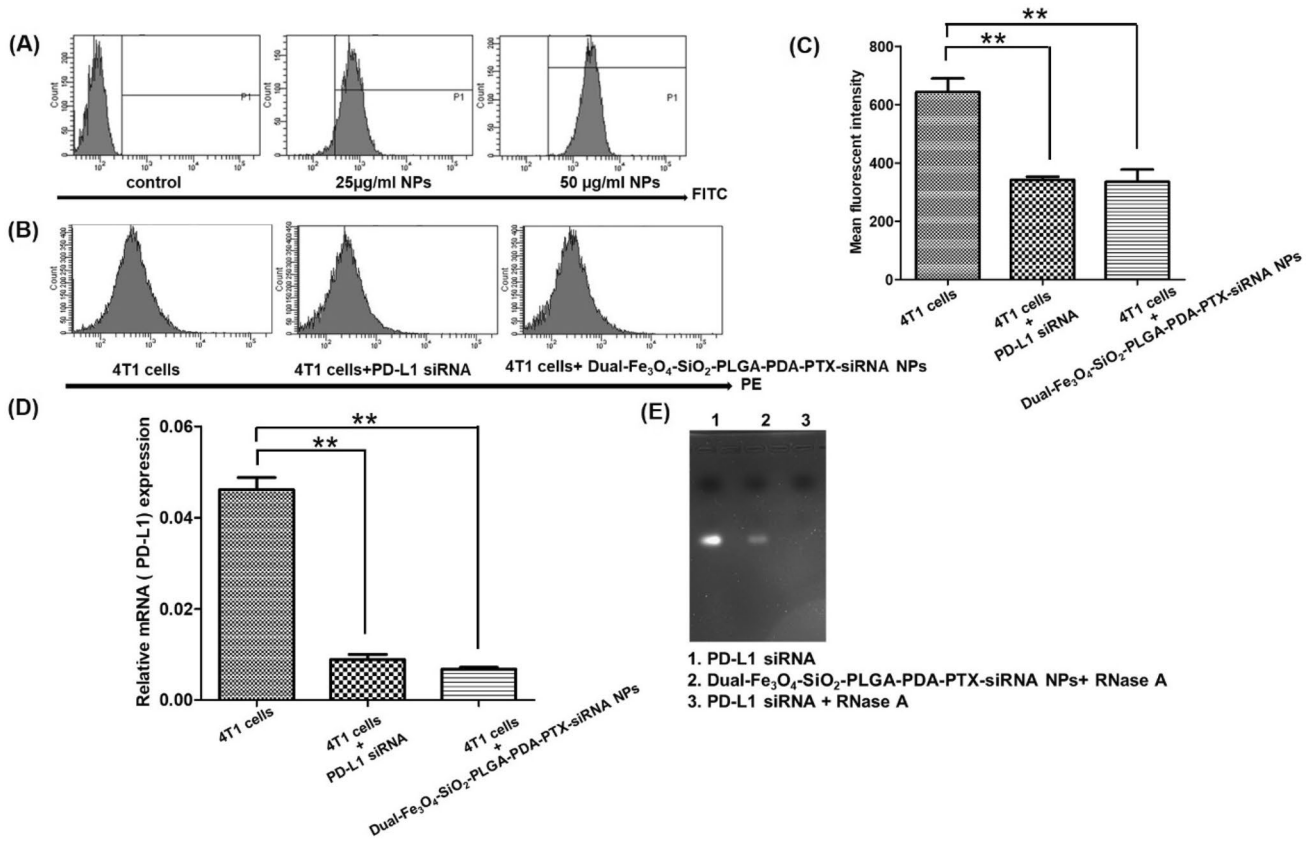

Fig. 4 **A** Cellular uptake studies, **B** dual-Fe3O4-SiO2-PLGA-PDA-PTX-siRNA NPs and PD-L1 siRNA-.mediated silencing of PD-L1 gene in 4T1 cells, **C** quantitative analysis showing significant decrease in mean fluorescent intensity of PD-L1 ($n=3$) ($p^{**}<0.001$), **D** qRT-PCR analysis showing significant reduction in relative mRNA expression of PD-L1 ($n=3$) ($p^{**}<0.001$), and **E** endonuclease protection assay. Data is represented as mean ± standard deviation. Statistical analysis was performed using one-way ANOVA followed by Bonferroni's post hoc comparison test

(*lane 3*), while a band for PD-L1 siRNA was observed with dual-Fe_3O_4-SiO_2-PLGA-PDA-PTX-siRNA NPs incubated with RNase-A (*lane 2*). These results signify that Fe_3O_4-SiO_2-PLGA-PDA-PTX-siRNA NPs protect PD-L1 against enzymatic digestion by RNase-A. PD-L1 siRNA without RNase treatment served as experimental control.

PD-L1 siRNA-loaded NP-mediated silencing of PD-L1 gene in 4T1 cells

Knockdown efficiency of dual-Fe_3O_4-SiO_2-PLGA-PDA-PTX-siRNA NPs in 4T1 cells were observed by flow cytometry and qRT-PCR analysis. Figure 4B shows the comparative knockdown analysis where dual-Fe_3O_4-SiO_2-PLGA-PDA-PTX-siRNA NPs significantly reduced the expression of PD-L1 receptor ($p^{**}<0.001$) with an equivalent efficiency to that of lipofectamine/PD-L1 siRNA. The mean fluorescent intensity of PD-L1 was observed as 643 ± 46.29 for control cells, 342.66 ± 10.06, and 335.33 ± 41.86 for cells treated with PD-L1 siRNA/lipofectamine and dual-Fe_3O_4-SiO_2-PLGA-PDA-PTX-siRNA NPs respectively (Fig. 4C). Quantitative RT-PCR results (Fig. 4D) also supported the flow cytometry observations where 4T1 cells treated with PD-L1 siRNA/lipofectamine and dual-Fe_3O_4-SiO_2-PLGA-PDA-PTX-siRNA NPs showed significant reduction in PD-L1 level ($p^{**}<0.001$) as compared to untreated cells.

Hemocompatibility study

In order to observe the biocompatibility of Fe_3O_4-SiO_2-PLGA-PDA-PTX-siRNA NPs with red blood cells, hemolysis assay was performed. Hemolysis study results showed that NPs at different concentrations from 25 to 200 µg/ml did not induce hemolysis similar to untreated RBCs, whereas RBCs incubated with 0.1% triton x-100 presented maximum RBCs lysis and served as a positive control (Fig. 5A). These results displayed that formulated nanoparticles did not show any significant toxicity towards RBCs, thereby these can be used safely for invivo therapeutic applications.

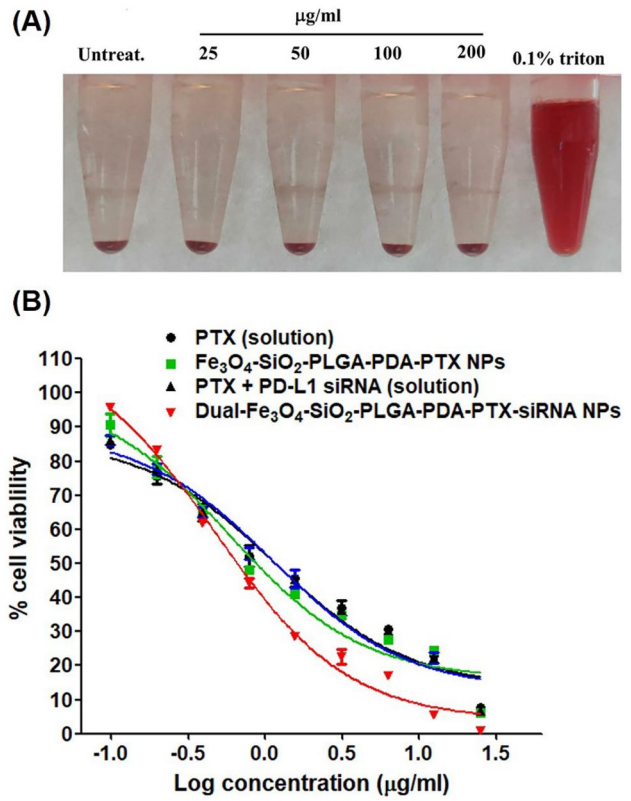

Fig. 5 **A** Hemolysis assay, RBCs incubated with dual-PTX + PD-L1siRNA, and dual-Fe_3O_4-SiO_2-PLGA-PDA-PTX-siRNA NPs at 25, 50, 100, and 200 μg/ml concentrations and 0.1% Triton X-100 (positive control). **B** MTT assay showing cytotoxic effect of PTX, Fe_3O_4-SiO_2-PLGA-PDA-PTX NPs, dual-PTX + PD-L1siRNA, and dual-Fe_3O_4-SiO_2-PLGA-PDA-PTX-siRNA NPs. Data is represented as mean ± standard deviation ($n = 3$)

In vitro cytotoxicity of PTX and PD-L1 siRNA-loaded nanoparticles

MTT assay was performed to determine the cytotoxicity of PTX, Fe_3O_4-SiO_2-PLGA-PDA-PTX NPs, PTX + PD-L1 siRNA in solution, and dual-Fe_3O_4-SiO_2-PLGA-PDA-PTX-siRNA NPs towards 4T1 cells (Fig. 5B). As expected, Fe_3O_4-SiO_2-PLGA-PDA-PTX NPs and PTX + PD-L1 siRNA in solution as well as dual-Fe_3O_4-SiO_2-PLGA-PDA-PTX-siRNA NPs presented dose-dependent killing of 4T1 cells following 48 h of treatment. Moreover, half-maximal inhibitory concentration (IC_{50}) was calculated as 1.159 μg/ml for PTX solution and 0.5898 μg/ml for Fe_3O_4-SiO_2-PLGA-PDA-PTX NPs, showing increased anti-cancer efficacy with NPs as compared to soluble PTX. PD-L1 siRNA did not itself show any significant cytotoxic effect on 4T1 cells, thereby PTX + PD-L1 siRNA in solution demonstrated almost similar efficacy as that of PTX solution and was found to be 1.120 μg/ml. The inclusion of siRNA in nanoparticles in combination to paclitaxel, i.e., dual-Fe_3O_4-SiO_2-PLGA-PDA-PTX-siRNA NPs have shown slight improvement in 4T1 cytotoxicity as compared to Fe_3O_4-SiO_2-PLGA-PDA-PTX NPs with an IC_{50} values calculated as 0.4705 μg/ml. It is known that downregulation of PD-L1 receptor in cancer cells helps in T cell-mediated tumor inhibition; hence, as expected, dual-Fe_3O_4-SiO_2-PLGA-PDA-PTX-siRNA NPs do not show any significant improvement over Fe_3O_4-SiO_2-PLGA-PDA-PTX NPs in the MTT assay in the absence of T cells.

Annexin V-FITC apoptosis assay

Figure 6 shows the apoptosis-inducing effect of PTX and Fe_3O_4-SiO_2-PLGA-PDA-PTX NPs on 4T1 cells after 24 h of treatment. Unstained and stained healthy cells were taken as experimental control (Supplementary Fig. S2). Treatment with Fe_3O_4-SiO_2-PLGA-PDA-PTX NPs and PTX solution showed 17.8 and 48.6% necrotic cells (Annexin V-FITC$^-$, PI$^+$, Q1 cells), respectively, while bare NPs maintained 92% cells viability (Annexin V-FITC$^-$, PI$^-$, Q3 cells), only 3% of cells was observed as dead cells (Fig. 6). These results clearly demonstrated that the necrosis effect observed with Fe_3O_4-SiO_2-PLGA-PDA-PTX NPs was mainly due to cytotoxic effect of drug. However, the Fe_3O_4-SiO_2-PLGA-PDA-PTX NPs showed less necrotic effect as compared to PTX-free drug solution after 24 h of treatment; this could be due to lesser availability of free drug with NPs because of sustained drug release effect with NPs as compared to drug solution. These results are supported by drug release data (Fig. 3), where only 20% of drug release was observed with Fe_3O_4-SiO_2-PLGA-PDA-PTX NPs in 24 h. Further, it could be anticipated that at later time points, higher efficacy may be observed with Fe_3O_4-SiO_2-PLGA-PDA-PTX NPs, as drug release from over a period of time will get increased as consistent with MTT data, where Fe_3O_4-SiO_2-PLGA-PDA-PTX NPs showed higher cytotoxicity as compared to free drug after 48 h of treatment (Fig. 5). PTX acts as antimicrotubule agents, thereby induces cell death mainly by inducing apoptosis pathway by activating caspase and cleaving poly (ADP-ribose) polymerase (PARP) [34]. Fe_3O_4-SiO_2-PLGA-PDA-siRNA NPs itself do not induce cell death (Fig. 6E), thereby the results are similar to control cells. However, treatment of cells with dual-Fe_3O_4-SiO_2-PLGA-PDA-PTX-siRNA NPs results in the activation of the apoptosis pathway with 8.1% cells (early apoptosis) and 11.7% necrotic cells (Fig. 6F), mainly due to PTX-induced apoptotic cell death.

Effect of PD-L1 knockdown on CD8$^+$ T cell proliferation

PD-1/PD-L1 pathway plays an important role in cancer immune escape by controlling and maintaining immune

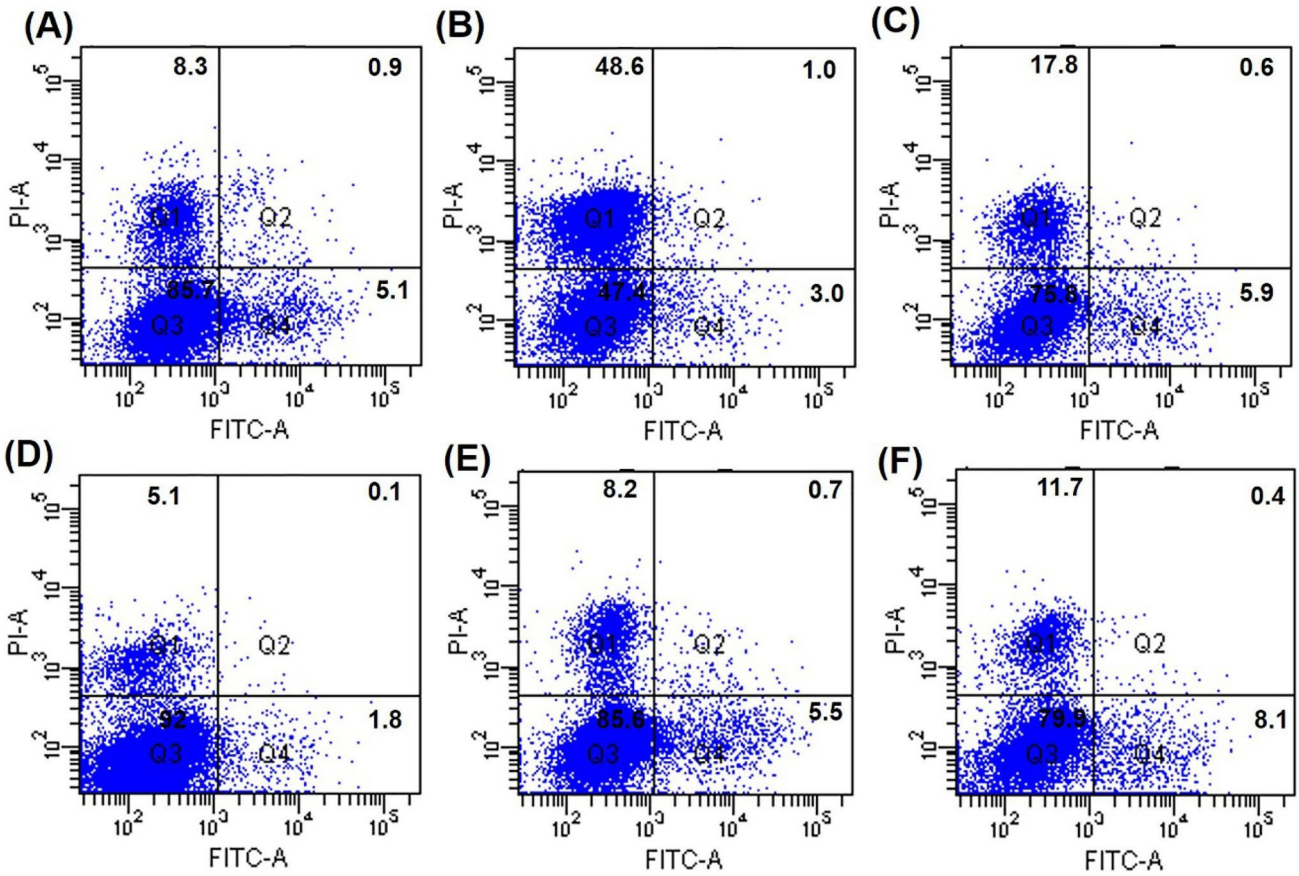

Fig. 6 Scatter plots of cells stained with annexin V/PI **A** control cells, cells treated with **B** PTX drug solution, **C** Fe_3O_4-SiO_2-PLGA-PDA-PTX NPs, **D** bare NPs, **E** Fe_3O_4-SiO_2-PLGA-PDA-siRNA NPs, **F** dual-Fe_3O_4-SiO_2-PLGA-PDA-PTX-siRNA NPs at 1 µg/ml concentration

tolerance within tumor microenvironment. Tumor-infiltrating T lymphocytes including cytotoxic $CD8^+$ T cells highly express the PD-1 receptor on the surface. Interaction of PD-1 receptor present on T cells with PD-L1 ligand present on tumor cells has been known to inhibit the T cell activation and suppresses the cytotoxic effect of $CD8^+$ T cells against cancer cells [35–37]. In this study, 4T1 cancer cells and splenocytes co-culture assay, it was observed that $CD3^+CD8^+$ T cells show higher proliferation following treatment of 4T1 cancer cells with Fe_3O_4-SiO_2-PLGA-PDA-siRNA NPs and dual-Fe_3O_4-SiO_2-PLGA-PDA-PTX-siRNA NPs as compared to untreated 4T1 cells. As compared to control cells, 9.87% $CD3^+CD8^+$ T cells showed proliferation, which was observed as decrease in CFSE-associated fluorescence with the appearance of small intensity peaks when the PD-L1 receptor were downregulated on 4T1 cells using Fe_3O_4-SiO_2-PLGA-PDA-siRNA NPs (Fig. 7D). Similarly, 10.72% $CD3^+CD8^+$ T cells were proliferative when the PD-L1 receptor were downregulated on 4T1 cells treated with dual-Fe_3O_4-SiO_2-PLGA-PDA-PTX-siRNA NPs (Fig. 7E). These observations suggested that PD-L1 downregulation on cancer cells has prevented the PD-1/PD-L1 interaction, and thus, cytotoxic $CD8^+$ T cells were able to proliferate more effectively in case of co-culture experiments with 4T1 cells treated with dual-Fe_3O_4-SiO_2-PLGA-PDA-PTX-siRNA NPs.

Tumor growth inhibition studies

Therapeutic efficacy of tumor-targeted combined chemo- and immunotherapy (dual-Fe_3O_4-SiO_2-PLGA-PDA-PTX-siRNA NPs) was evaluated in tumor-bearing mice. Tumor growth inhibition was monitored by calculating the tumor volume, where PTX and dual-Fe_3O_4-SiO_2-PLGA-PDA-PTX-siRNA NPs led to tumor regression as compared to untreated mice and mice treated with bare NPs. Moreover, dual-Fe_3O_4-SiO_2-PLGA-PDA-PTX-siRNA NPs were significantly more effective than Fe_3O_4-SiO_2-PLGA-PDA-PTX NPs in inhibiting tumor growth (Fig. 8A). Bare NPs did not show any therapeutic effect. These results concluded that a combined treatment strategy via dual-Fe_3O_4-SiO_2-PLGA-PDA-PTX-siRNA NPs has remarkable anti-cancer therapeutic potential as compared to chemotherapy with Fe_3O_4-SiO_2-PLGA-PDA-PTX NPs alone.

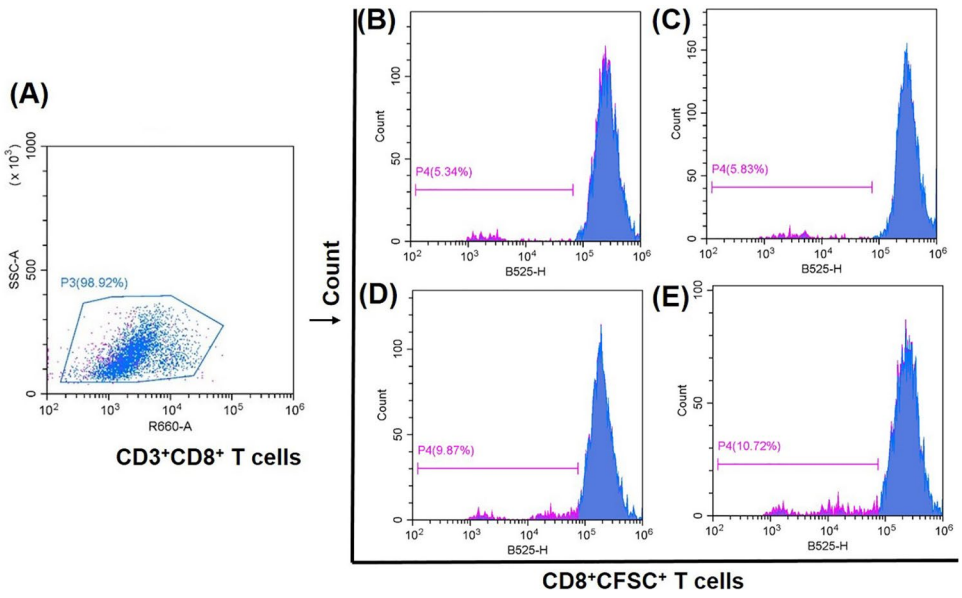

Fig. 7 $CD3^+CD8^+$ T cells proliferation was analyzed using CFSE dilution by flow cytometry, 4T1 cells treated with different anti-PD-L1 siRNA NPs were co-cultured for 48 h with splenocytes primed against the 4T1 cells and analyzed using flow cytometer **A** $CD3^+CD8^+$ positive cells (gated), **B** control $CD3^+CD8^+$ T cells, co-cultured cells treated with **C** Fe_3O_4-SiO_2-PLGA-PDA-NPs, **D** Fe_3O_4-SiO_2-PLGA-PDA-siRNA NPs, **E** dual-Fe_3O_4-SiO_2-PLGA-PDA-PTX-siRNA NPs

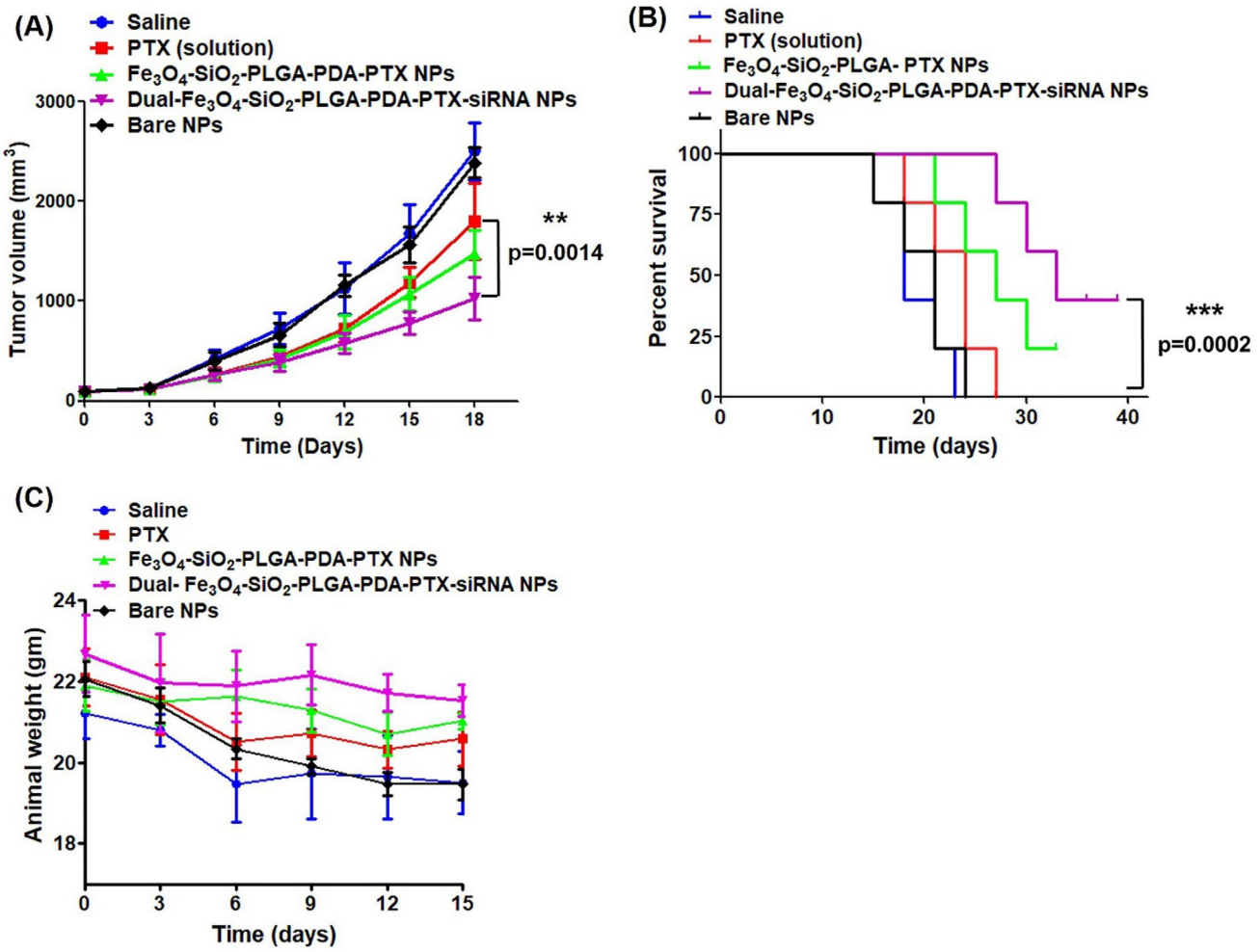

Fig. 8 In vivo animal studies showing effect of PTX, Fe_3O_4-SiO_2-PLGA-PDA-PTX NPs and dual-Fe_3O_4-SiO_2-PLGA-PDA-PTX-siRNA NPs on **A** tumor inhibition over a period of time (mean tumor volume at day 18 was considered for significance, $p = 0.0014$, **B** percentage animal survival as analysed using Kaplan-Meier survival curve ($p = 0.0002$), **C** changes in animal body weight with time and (mean ± standard deviation, $n = 5$)

Mechanistic explanation of increased therapeutic efficacy observed with dual-Fe_3O_4-SiO_2-PLGA-PDA-PTX-siRNA NPs against breast cancer is given here. PTX leads to cancer cell death by inducing microtubule stabilization. Thereby, Fe_3O_4-SiO_2-PLGA-PDA-PTX NPs guarantee sustained availability of PTX within the cells for a sufficient longer period of time in a pH-dependent manner, and demonstrate increased cancer cell killing and reduced PTX-mediated side effects as compared to PTX drug solution. Later, these necrotic and late apoptotic cancer cells release cancer-specific antigen, that are presented to cytotoxic T cells through MHC-I and II pathway by antigen-presenting cells (APCs), which results in generation of cancer antigen-specific cytotoxic T cells. These antigenic cytotoxic T cells are capable to kill cancer cells upon recognizing the cognate antigen present on tumor cells; however, higher expression of PD-L1 protein on the cancer cells engages the PD-1 receptor present on cancer antigen-specific cytotoxic T cells and converts them to tolerogenic T cells. As a consequence, these tolerogenic T cells lost the capability of cancer cell killing and generate an immunosuppressive environment. In such case, downregulating PD-L1 receptor on cancer cells emerged as a promising treatment approach to potentiate PTX-mediated cancer cell death.

Thereby, in this report, co-delivery of anti-PD-L1 siRNA using dual-Fe_3O_4-SiO_2-PLGA-PDA-PTX-siRNA NPs has demonstrated increased cancer cell killing efficacy compared to Fe_3O_4-SiO_2-PLGA-PDA-PTX NPs. Dual-Fe_3O_4-SiO_2-PLGA-PDA-PTX-siRNA NPs not only significantly inhibited the tumor growth (mean tumor volume), but also significantly improved the animal survival (Fig. 8A and B). In addition, dual-Fe_3O_4-SiO_2-PLGA-PDA-PTX-siRNA NPs have improved the animal weight (non-significant) as compared to PTX alone (Fig. 8C). Bare NPs neither improved the animal survival nor body weight. Hence, co-delivery of PTX and PD-L1 siRNA using pH-triggered polymer PLGA-coated core–shell magnetic silica nanoparticles may have a promising anti-cancer treatment potential, where PTX directly kills the cancer cells, and PD-L1 siRNA maintains the functional potential of cytotoxic T cells.

Conclusion and future perspectives

Combined chemotherapy along with immunotherapy via dual-Fe_3O_4-SiO_2-PLGA-PDA-PTX-siRNA NPs leads to PTX-mediated cell death along with increased sensitivity of cancer cells towards cytotoxic T cells via PD-L1 knockdown and inhibition of immune escape mechanism. Thus, developed dual-PTX + PD-L1 siRNA-loaded Fe_3O_4-SiO_2-PLGA-PDA-PTX-siRNA NPs were ~ 230 nm in size, spherical in shape, suitable for cancer cell targeting by enhanced permeability and retention (EPR) effect. PTX-loaded NPs showed sustained PTX release up to 10 days. Flow cytometry results presented efficient internalization of nanoparticles by 4 T1 cells and PD-L1 gene down-regulation. The nanoparticles were also capable to provide endonuclease protection to entrapped PD-L1 siRNA. Furthermore, dual-Fe_3O_4-SiO_2-PLGA-PDA-PTX-siRNA NPs presented excellent hemocompatibility. Tumor regression studies conducted in vivo reported significant inhibition of tumor growth in animals treated with dual-Fe_3O_4-SiO_2-PLGA-PDA-PTX-siRNA NPs as compared to animals treated with Fe_3O_4-SiO_2-PLGA-PDA-PTX NPs. Thus, the selective gene silencing of PD-L1 siRNA along with paclitaxel chemotherapy via three-layered nanosystem: first, core-shell iron oxide silica; second, polymer PLGA functionalization; and third, pH-stimuli based "on demand" drug release, i.e., PDA capping may emerge as therapeutic opportunity to treat cancer displaying abnormal expression of PD-L1 gene with high anti-cancer efficacy. Furthermore, the synergy observed between chemotherapy and immunotherapeutic exploited for enhancing anti-tumor response may open the way to develop other advanced combination therapies employing targeted delivery systems. Furthermore, taking advantage of inorganic core materials, multimodal therapies can be explored. In one such example, nitric oxide and doxorubicin delivery using sodium alginate microspheres (BND-MSs) in combination of photothermal therapy were attempted which resulted in suppression of tumor growth [38]. Likewise, the developed nanosystem dual-Fe_3O_4-SiO_2-PLGA-PDA-PTX-siRNA NPs can be exploited in future, where magnetic core (Fe_3O_4)-induced magnetic hyperthermia-mediated cancer cell death [39] can be exploited in with combined chemo-immunotherapy. Furthermore, some experiments related to alteration in magnetic field mediated nanoparticle targeting and drug release may be performed to enhance anti-cancer therapeutic efficacy.

Supplementary methods

Synthesis of pH-responsive PLGA-coated core-shell magnetic silica nanoparticle

In brief, iron oxide nanoparticles (Fe_3O_4) were prepared by co-precipitation of iron (II) and iron (III) chloride salts under N2 atmosphere using 2M NaOH [26]. Initially, the iron salts were dissolved in the 50 ml of water in the molar ratio of 2:1, then NaOH was added slowly and the reaction temperature was raised to 70 °C. After 3h, the reaction was cooled down and the Fe_3O_4 was collected with the help of magnet and vacuum dried.

In the second step, core-shell magnetic silica nanoparticles were prepared by modified sol-gel homogenous co-precipitation process [27]. Fe_3O_4 NPs were dispersed in a

mixture of ethanol and water (80:20). Tetra ethyl ortho silicate (TEOS), 0.1 ml (0.1% w/v) was added to the magnetic nanoparticles and stirred for 10 min at room temperature. Then, 2M NaOH (1 ml) was added slowly and reaction mixture was stirred for 6 h at room temperature. The core-shell magnetic silica nanoparticles (Fe_3O_4-SiO_2 NPs) were separated using an external magnet, washed with deoxygenated distilled water and vacuum dried. To achieve amine functionalization, Fe_3O_4-SiO_2 NPs were dispersed in pure ethanol and 2 mmol, 3-aminopropyl triethoxysilane (APTES) was added to it, refluxed at 70 °C, washed with ethanol two-three times and vacuum dried.

In the third step, PLGA-coated Fe_3O_4-SiO_2 nanoparticles were prepared by double emulsion solvent evaporation method [28]. Poly lactic co-glycolic acid (PLGA) was dissolved in dichloromethane (DCM). Fe_3O_4-SiO_2 NPs were dispersed in 0.5 ml of 1% PVA solution and added to PLGA solution with probe sonication (30% amplitude, 20 duty cycles, 2 min) to form primary emulsion (W_1/O). The ratio of Fe_3O_4-SiO_2 nanoparticles to PLGA was optimized as 1:1. Thus formed primary emulsion was then added to 30 ml of 2% PVA solution with sonication (30% amplitude, 20 duty cycles, 3 min) to form double emulsion (W_1/O/W_2) and continuously stirred for 5 h to evaporate DCM. After 5 h, PLGA-coated nanoparticles designated as Fe_3O_4-SiO_2-PLGA were collected using external magnet, washed and dried.

In the fourth step, in order to fabricate pH-sensitive release system, PLGA-coated Fe_3O_4-SiO_2 nanoparticles (100 mg) were dispersed in 10 ml of dopamine hydrochloride solution in Tris-HCl buffer (10 mmol/L, pH 8.5) and continuous stirred for 6 h at room temperature [29]. After 6 h, poly dopamine (PDA) capped nanoparticles designated as Fe_3O_4-SiO_2-PLGA-PDA NPs/bare NPs were separated with magnet, washed with water, lyophilized and stored for further use.

Supplementary Information The online version contains supplementary material available at https://doi.org/10.1007/s13346-024-01521-0.

Author contribution Dr. JM, Dr. AG, and Dr. AKP have conceptualized and designed the study. Dr. AG has performed the experiments and has written the manuscript, MS performed hemolysis studies, Dr. VK performed flow cytometry experiments, KN performed the survival study, and HC performed the graphical abstract drawing and proof reading. All the authors have approved the manuscript for submission and publication.

Funding This work was supported by ICMR grant-File no. 5/3/8/39/ITR-F/2019 and SERB NPDF grant-File no. PDF/2022/003287 which was received by Dr. Anuradha Gupta.

Data availability All the materials used in the manuscript are commercially available; however, 4T1 cells can be requested from Prof. Avinash Bajaj, Regional Centre of Biotechnology, Faridabad, India. Data required for results and conclusion has included in the manuscript however, raw data will be provided by the corresponding author on reasonable request.

Declarations

Ethics approval This study was performed as per the institutional animal ethical guideline after approval from the Animal Ethical Committee of National Institute of Immunology (IAEC#500/19), New Delhi, India.

Conflict of interest The authors declare no competing interests.

References

1. Bailly C, Thuru X, Quesnel B. Combined cytotoxic chemotherapy and immunotherapy of cancer: modern times. NAR Cancer. 2020 Feb 17;2(1):zcaa002. https://doi.org/10.1093/narcan/zcaa002. PMID: 34316682; PMCID: PMC8209987.
2. Marupudi NI, et al. Paclitaxel: a review of adverse toxicities and novel delivery strategies. Expert Opin Drug Saf. 2007;6(5):609–21.
3. Chou PL, Huang YP, Cheng MH, Rau KM, Fang YP. Improvement of Paclitaxel-Associated Adverse Reactions (ADRs) via the Use of Nano-Based Drug Delivery Systems: A Systematic Review and Network Meta-Analysis. Int J Nanomedicine. 2020 Mar 12;15:1731–1743. https://doi.org/10.2147/IJN.S231407. PMID: 32210563; PMCID: PMC7075337.
4. Zhang H, et al. Iridium oxide nanoparticles-based theranostic probe for in vivo tumor imaging and synergistic chem/photothermal treatments of cancer cells. Chem Eng J. 2022;430:132675.
5. Zhou Y, et al. Upconverting nanoparticles based nanodevice for DNAzymes amplified miRNAs detection and artificially controlled chemo-gene therapy. Biosens Bioelectron. 2022;214:114549.
6. Qiu L, et al. A targeted, self-delivered, and photocontrolled molecular beacon for mRNA detection in living cells. J Am Chem Soc. 2013;135(35):12952–5.
7. Yan J, et al. Therapeutic DNAzymes: from structure design to clinical applications. Adv Mater. 2023: p. 2300374.
8. Mueller SN, et al. PD-L1 has distinct functions in hematopoietic and nonhematopoietic cells in regulating T cell responses during chronic infection in mice. J Clin Investig. 2010;120(7):2508–15.
9. Bartlett DW, Davis ME. Effect of siRNA nuclease stability on the in vitro and in vivo kinetics of siRNA-mediated gene silencing. Biotechnol Bioeng. 2007;97(4):909–21.
10. Volkov AA, et al. Selective protection of nuclease-sensitive sites in siRNA prolongs silencing effect. Oligonucleotides. 2009;19(2):191–202.
11. Lee JM, Yoon TJ, Cho YS. Recent developments in nanoparticle-based siRNA delivery for cancer therapy. Biomed Res Int. 2013;2013:782041. https://doi.org/10.1155/2013/782041. Epub 2013 Jun 17. PMID: 23844368; PMCID: PMC3703404.
12. Tomar RS, Matta H, Chaudhary PM. Use of adeno-associated viral vector for delivery of small interfering RNA. Oncogene. 2003;22(36):5712–5.
13. Thomas CE, Ehrhardt A, Kay MA. Progress and problems with the use of viral vectors for gene therapy. Nat Rev Genet. 2003;4(5):346–58.
14. Emens LA, Middleton G. The interplay of immunotherapy and chemotherapy: harnessing potential synergies. Cancer Immunol Res. 2015;3(5):436–43.
15. Hanoteau A, Moser M. Chemotherapy and immunotherapy: a close interplay to fight cancer? Oncoimmunology. 2016;5(7):e1190061.

16. Attia MF, et al. An overview of active and passive targeting strategies to improve the nanocarriers efficiency to tumour sites. J Pharm Pharmacol. 2019;71(8):1185–98.
17. Zhang Y, Cao J, Yuan Z. Strategies and challenges to improve the performance of tumor-associated active targeting. J Mater Chem B. 2020;8(18):3959–71.
18. Thiramanas R, et al. Cellular uptake of siRNA-loaded nanocarriers to knockdown PD-L1: strategies to improve T-cell functions. Cells. 2020;9(9):2043.
19. Wu Y, et al. Silencing PD-1 and PD-L1 with nanoparticle-delivered small interfering RNA increases cytotoxicity of tumor-infiltrating lymphocytes. Nanomedicine. 2019;14(8):955–67.
20. Islam T, Josephson L. Current state and future applications of active targeting in malignancies using superparamagnetic iron oxide nanoparticles. Cancer Biomark. 2009;5(2):99–107.
21. Chen L, et al. Magnetic targeting combined with active targeting of dual-ligand iron oxide nanoprobes to promote the penetration depth in tumors for effective magnetic resonance imaging and hyperthermia. Acta Biomater. 2019;96:491–504.
22. Palanisamy S, Wang YM. Superparamagnetic iron oxide nanoparticulate system: synthesis, targeting, drug delivery and therapy in cancer. Dalton Trans. 2019;48(26):9490–515.
23. Zhang MW, et al. Controlled fabrication of iron oxide/mesoporous silica core-shell nanostructures. J Phys Chem C. 2013;117(41):21529–38.
24. Gupta A, et al. Nanocarrier composed of magnetite core coated with three polymeric shells mediates LCS-1 delivery for synthetic lethal therapy of BLM-defective colorectal cancer cells. Biomacromol. 2018;19(3):803–15.
25. Ahmad A, et al. Hyperbranched polymer-functionalized magnetic nanoparticle-mediated hyperthermia and niclosamide bimodal therapy of colorectal cancer cells. ACS Biomater Sci Eng. 2020;6(2):1102–11.
26. Hariani PL, et al. Synthesis and properties of Fe3O4 nanoparticles by co-precipitation method to removal procion dye. Int J Environ Sci Dev. 2013;4(3):336–40.
27. Tang H, et al. Facile synthesis of pH sensitive polymer-coated mesoporous silica nanoparticles and their application in drug delivery. Int J Pharm. 2011;421(2):388–96.
28. Saini K, Bandyopadhyaya R. Transferrin-conjugated polymer-coated mesoporous silica nanoparticles loaded with gemcitabine for killing pancreatic cancer cells. ACS Applied Nano Materials. 2019;3(1):229–40.
29. Wei Y, et al. Polydopamine and peptide decorated doxorubicin-loaded mesoporous silica nanoparticles as a targeted drug delivery system for bladder cancer therapy. Drug Delivery. 2017;24(1):681–91.
30. Chan A, et al. Remote and local control of stimuli responsive materials for therapeutic applications. Adv Drug Deliv Rev. 2013;65(4):497–514.
31. Hernández-Hernández AA, et al. Iron oxide nanoparticles: synthesis, functionalization, and applications in diagnosis and treatment of cancer. Chem Pap. 2020;74(11):3809–24.
32. Makadia HK, Siegel SJ. Poly lactic–glycolic acid (PLGA) as biodegradable controlled drug delivery carrier. Polymers. 2011;3(3):1377–97.
33. Goyal AK, et al. Application and perspective of pH-responsive nano drug delivery systems. In: Applications of Targeted Nano Drugs and Delivery Systems. Elsevier; 2019. p. 15–33.
34. Khing TM, et al. The effect of paclitaxel on apoptosis, autophagy and mitotic catastrophe in AGS cells. Sci Rep. 2021;11(1):23490.
35. Callahan MK, Postow MA, Wolchok JD. Targeting T cell co-receptors for cancer therapy. Immunity. 2016;44(5):1069–78.
36. Han Y, Liu D, Li L. PD-1/PD-L1 pathway: current researches in cancer. Am J Cancer Res. 2020;10(3):727.
37. Chen S, et al. Combination of 4–1BB agonist and PD-1 antagonist promotes antitumor effector/memory CD8 T cells in a poorly immunogenic tumor model. Cancer Immunol Res. 2015;3(2):149–60.
38. Liang D, Kuang G., Chen X., Lu J., Shang L., Sun W. Near-infrared light-responsive Nitric oxide microcarrier for multimodal tumor therapy. Smart Medicine. 2023, 2(3), e20230016. https://doi.org/10.1002/SMMD.20230016.
39. Fernandes S, et al. Magnetic nanoparticle-based hyperthermia mediates drug delivery and impairs the tumorigenic capacity of quiescent colorectal cancer stem cells. ACS Appl Mater Interfaces. 2021;13(14):15959–72.